

06,11

Investigation of the magnetoelectric effect and thermoelectric power of the composite of iron-substituted bismuth pyrostannate $\text{Bi}_2(\text{Sn}_{0.7}\text{Fe}_{0.3})_2\text{O}_7/\text{Bi}_2\text{Fe}_4\text{O}_9$

© L.V. Udod^{1,2}, S.S. Aplesnin^{1,2}, M.N. Sitnikov², O.B. Romanova¹

¹ Kirensky Institute of Physics of Federal Research Center KSC of the Siberian Branch of RAS, Krasnoyarsk, Russia

² Siberian State University of Science and Technology, Krasnoyarsk, Russia

E-mail: luba@iph.krasn.ru

Received May 15, 2023

Revised May 15, 2023

Accepted June 3, 2023

The composite compound $\text{Bi}_2(\text{Sn}_{0.7}\text{Fe}_{0.3})_2\text{O}_7/\text{Bi}_2\text{Fe}_4\text{O}_9$ in the ratio 91/9% was synthesized by the solid-phase reaction method. The current-voltage characteristics were studied in the temperature range 800–400 K. The hysteresis of the current-voltage characteristics was found. The magnetoelectric interaction and thermoelectric power have been studied. The temperatures of predominance of the even and linear functions of the magnetoelectric effect are established. The sign change of the thermopower has been found.

Keywords: composite, magnetoelectric effect, current-voltage characteristics, hysteresis, thermoelectric power.

DOI: 10.61011/PSS.2023.08.56576.83

1. Introduction

The new generation of materials in demand in modern devices was the reason for the intensive study of multiferroics and ferroelectrics. The mutual influence of the magnetic and electrical subsystems leads to the manifestation of the magnetoelectric effect. In multiferroics, induced magnetization occurs in the applied electric fields and electric polarization occurs in an external magnetic field. Magnetoelectric interaction has been established in ceramic materials based on bismuth ferrite $(\text{BiFeO}_3)_{1-x}-(\text{BaTiO}_3)_x$, $\text{Bi}_{1-x}\text{Nd}_x\text{FeO}_3$ and $\text{Bi}_5\text{Ti}_3\text{FeO}_{15}$. The highest value of the magnetoelectric coupling coefficient (α_{ME}) was obtained for the connection $\text{Bi}_5\text{Ti}_3\text{FeO}_{15}$ ($\alpha_{\text{ME}} \sim 10 \text{ mV cm}^{-1}\text{Oe}^{-1}$). In the case of solid solutions $(\text{BiFeO}_3)_{1-x}-(\text{BaTiO}_3)_x$ and $\text{Bi}_{1-x}\text{Nd}_x\text{FeO}_3$ maximum α_{ME} has order 1 and $2.7 \text{ mV cm}^{-1}\text{Oe}^{-1}$ respectively. The magnitude of the magnetoelectric coupling depends on the structure of solid solutions. The magnetoelectric effect (ME effect) is found in the compound $\text{Bi}_5\text{Ti}_3\text{FeO}_{15}$ without long-range magnetic order. In the case of solid solutions $(\text{BiFeO}_3)_{1-x}-(\text{BaTiO}_3)_x$ and $\text{Bi}_{1-x}\text{Nd}_x\text{FeO}_3$ the ME effect appears after suppression of the cycloidal spin structure of BiFeO_3 . The magnitude of the magnetoelectric coupling depends on the concentration of barium titanate and neodymium in the structure of bismuth ferrite. The maximum values of the magnetoelectric coupling coefficient were obtained for compositions in the region of structural transformations [1].

The magnetoelectric effect is used in magnetic field sensors [2–4], energy collection devices [5–7], new generation memory [8–10], spintronics devices (for example,

spin valves, magnetic tunnel junctions) [11–13], microwave devices, millimeter-wave devices and miniature antennas [7], as well as in wireless medical instruments (for example, for endoscopy and brain imaging) [7]. The implementation of such innovative devices requires the development of materials with the highest possible magnetoelectric coupling coefficient.

The synthesis of new single-phase multiferroics with a high value of the magnetoelectric coupling coefficient is a difficult task. So far, the most recognized single-phase multiferroic compound is bismuth ferrite BiFeO_3 , in which ferroelectric and antiferromagnetic ordering coexist at ambient temperature (Neel antiferromagnetic temperature $T_N = 643 \text{ K}$, Curie ferroelectric temperature $T_C = 1100 \text{ K}$) [14]. However, due to the cycloidal modulation of the spin arrangement, a linear magnetoelectric effect is not observed in bulk polycrystalline bismuth ferrite. In BiFeO_3 thin films with the disappearance of the spin cycloid, a giant magnetoelectric coupling was observed, $\alpha_{\text{ME}} \sim 3 \text{ V cm}^{-1}\text{Oe}^{-1}$ [15].

The magnetoelectric effect is especially great in composite materials. In dispersed composites such as $\text{BaTiO}_3/\text{CoFe}_2\text{O}_4$, $\text{PbZr}_{1-x}\text{Ti}_x\text{O}_3$ (PZT)/ $\text{Tb}_{1-x}\text{Dy}_x\text{Fe}_2$ (terphenol-D) and $\text{Ba}_{0.8}\text{Pb}_{0.2}\text{TiO}_3/\text{CuFe}_{1.8}\text{Cr}_{0.2}\text{O}_4$ value α_{ME} order $100\text{--}130 \text{ mV cm}^{-1}\text{Oe}^{-1}$ [16]. Multilayer composites also demonstrate a greater value of α_{ME} , for example, in PZT/Terphenol-D laminates α_{ME} reaches $\sim 4.7 \text{ mV cm}^{-1}\text{Oe}^{-1}$ [17] and $90 \text{ mV cm}^{-1}\text{Oe}^{-1}$ in laminated composites PZT/Permendur [18]. Magnetoelectric coupling is also observed in nanostructured multiferroic ceramic materials (for example, YMnO_3 [19]), semiconductor

membranes galvanically filled with magnetostrictive material (for example, InP membrane, filled with Ni [20]), as well as in thin nanocomposite films (for example, CoFe_2O_4 [21]).

Composite materials that include various phases the properties of which change during deformation are of particular interest. For example, composites containing magnetic (ferro- or ferrimagnetic material) and ferroelectric. Magnetostrictive deformation occurs in magnetic materials under the influence of an external magnetic field, and ferroelectric materials have a piezoelectric effect. The interaction of composite components through deformation at their interface leads to the appearance of the magnetoelectric effect [22].

$\text{Bi}_2\text{Fe}_4\text{O}_9$ belongs to the class of mullite-like compounds and exhibits properties of multiferroics, paramagnetic at room temperature. The crystal structure is orthorhombic *Pbam* [23]. Intensive study of mullite in recent years is due to its wide application, such as semiconductor gas sensors and as a catalyst in the oxidation of ammonium [24,25]. The physical properties of $\text{Bi}_2\text{Fe}_4\text{O}_9$ depend on the method of production and grain size [26]. The volumetric $\text{Bi}_2\text{Fe}_4\text{O}_9$ obtained by solid-phase synthesis detects a ferroelectric hysteresis loop at 250 K and antiferromagnetic ordering at 260 K [27], which indicates about multiferroic properties.

Electrical polarization at room temperature detects hysteresis loops with rounded ends. Rounded ends occur due to large leakage currents [26]. Samples with a grain size greater than 200 nm at room temperature have unsaturated hysteresis loops [28]. So, a sample with a grain size of 900 nm has a residual polarization of $P_r = 0.21 \text{ C/cm}^2$ and a coercive force of $E_c = 19.5 \text{ kV/cm}$ in a field of 60 kV/cm. These data indicate ferroelectric properties. In addition, this sample has the lowest leakage current density 10^{-6} A/cm^2 and the highest residual polarization 0.21 C/cm^2 [26].

Leakage currents are greatly reduced in samples with a grain size greater than 200 nm and are also characterized by a ferroelectric hysteresis loop at room temperature. Ceramic and nano-crystalline samples $\text{Bi}_2\text{Fe}_4\text{O}_9$ detect the magnetodielectric effect [29].

Bismuth pyrostannate $\text{Bi}_2\text{Sn}_2\text{O}_7$ is a dielectric and at room temperature belongs to a monoclinic structure (α -phase) with a space group *P1c1* [30]. The substitution of tin with iron in $\text{Bi}_2\text{Sn}_2\text{O}_7$ does not change the spatial group, but leads to magnetic ordering. As a result of the interaction between the magnetic and ferroelectric subsystems, a magnetoelectric effect occurs [31]. For $\text{Bi}_2(\text{Sn}_{0.9}\text{Fe}_{0.1})_2\text{O}_7$, the electric polarization is a linear function of the electric field. A hysteresis of migration-type electrical polarization and a magnetoelectric effect were detected in bismuth pyrostannate with an increase of the concentration of iron ions for $x = 0.2$. The nonlinear behavior of magnetization in magnetic fields up to 50 kOe in the paramagnetic state at temperatures up to 200 K is associated with the magnetoelectric interaction. The electric polarization induced by the magnetic field is an even function of the magnetic field, with the exception

of the structural phase transition region, where the linear magnetoelectric effect [31] prevails.

When developing methods for the synthesis of multiferroics (MF) and a possible way to improve ME properties, it is necessary to solve two problems. First, find ways to get MF. Secondly, it is necessary to select certain structural and magnetic parameters of the crystal lattice that lead to the appearance of the ME effect in bulk samples. The ME properties of bulk samples can be improved by applying strong magnetic fields or very high mechanical stresses [32]. However, a similar result can be obtained by partial substitution of cations or the creation of a composite compound, which is analogous to mechanical pressure on the crystal lattice, which in a certain way changes the structure of the compound and allows to obtain the values of the ME effect by an order of magnitude higher than [33].

In this regard, the composite compound $\text{Bi}_2(\text{Sn}_{0.7}\text{Fe}_{0.3})_2\text{O}_7/\text{Bi}_2\text{Fe}_4\text{O}_9$ is of great interest, in which the ME effect is supposed to be detected.

The purpose of this work is to study the mutual influence of various crystallographic and magnetic structures $\text{Bi}_2(\text{Sn}_{0.7}\text{Fe}_{0.3})_2\text{O}_7$ and $\text{Bi}_2\text{Fe}_4\text{O}_9$ on the magnetoelectric effect and thermal EMF.

2. Samples and experimental methods

Composite compound $\text{Bi}_2(\text{Sn}_{0.7}\text{Fe}_{0.3})_2\text{O}_7/\text{Bi}_2\text{Fe}_4\text{O}_9$ (BSFO/BFO) was synthesized by the solid-phase reaction method. This method is widely used for the production of polycrystalline bulk materials, and also provides a wide selection of starting materials, such as oxides. The advantage of solid-phase synthesis is that solid reagents react chemically at high temperature in the absence of any solvent, resulting in a stable product. Fine powders of oxides Bi_2O_3 , SnO_2 , Fe_2O_3 were used as initial reagents. The stoichiometric mixture of the initial components was thoroughly ground in an agate mortar with ethyl alcohol until a homogeneous state was achieved. The charge was pressed at room temperature and annealed at temperatures 800–950°C in several stages. Annealing is used for controlling structural changes, properties and phase composition. According to X-ray structural data, the synthesized composite contains $\text{Bi}_2(\text{Sn}_{0.7}\text{Fe}_{0.3})_2\text{O}_7$ — 91% and $\text{Bi}_2\text{Fe}_4\text{O}_9$ — 9%. The powder X-ray was taken on a Bruker D8 ADVANCE diffractometer at room temperature. A linear detector of VANTEC and $\text{CuK}\alpha$ -radiation were used in this experiment. Bismuth pyrostannate $\text{Bi}_2(\text{Sn}_{0.7}\text{Fe}_{0.3})_2\text{O}_7$ corresponds to a monoclinic cell *Pc* in the α -phase $\text{Bi}_2\text{Sn}_2\text{O}_7$ [31], $\text{Bi}_2\text{Fe}_4\text{O}_9$ — orthorhombic structure *Pbam* [34]. The initial structures of these phases were used to refine the structure by the Rietveld method. The refinement was implemented using the TOPAS 4.2 [35] program and gave low R-factors of unreliability (table, Fig. 1).

Morphological studies, qualitative and semi-quantitative elementary composition were performed on the Scanning

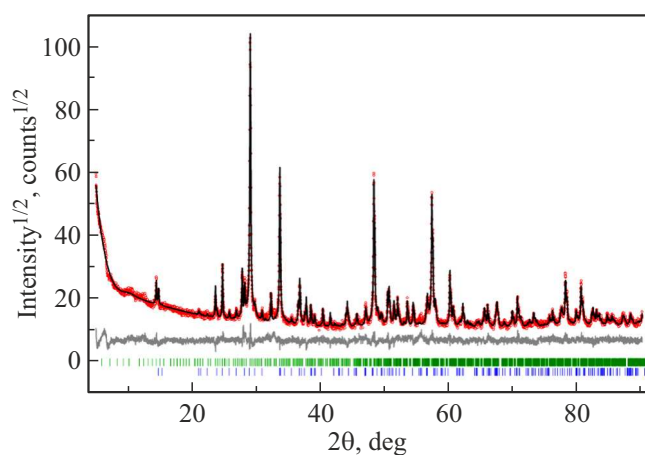


Figure 1. X-ray diffraction patterns of $\text{Bi}_2(\text{Sn}_{0.7}\text{Fe}_{0.3})_2\text{O}_7/\text{Bi}_2\text{Fe}_4\text{O}_9$.

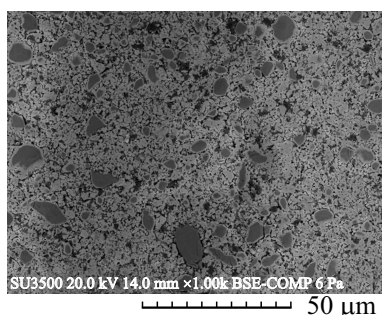


Figure 2. Micrography of $\text{Bi}_2(\text{Sn}_{0.7}\text{Fe}_{0.3})_2\text{O}_7/\text{Bi}_2\text{Fe}_4\text{O}_9$.

electron microscope (SEM) Hitachi S5500 on the argon-polished surface of the sample. The scanning was conducted in various micro-regions of the sample and gives the identity of the results. Analysis of the BSFO/BFO composite micrograph (Fig. 2) showed a dense, uneven distribution of grains $\text{Bi}_2\text{Fe}_4\text{O}_9$ surrounded by a matrix $\text{Bi}_2(\text{Sn}_{0.7}\text{Fe}_{0.3})_2\text{O}_7$ and the presence of pores. Grain shape $\text{Bi}_2\text{Fe}_4\text{O}_9$ in the form of dark-colored plates with truncated corners and

Parameters of the crystal structure of the composite compound $\text{Bi}_2(\text{Sn}_{0.7}\text{Fe}_{0.3})_2\text{O}_7/\text{Bi}_2\text{Fe}_4\text{O}_9$

Spatial group	$\text{Bi}_2\text{Fe}_4\text{O}_9$	$\text{Bi}_2(\text{Sn}_{0.7}\text{Fe}_{0.3})_2\text{O}_7$
	<i>Pbam</i>	<i>Pc</i>
<i>a</i> , Å	7.96795 (2)	15.0927 (5)
<i>b</i> , Å	8.45160 (3)	15.0830 (5)
<i>c</i> , Å	6.01100 (2)	21.3150 (8)
β , °	90 (2)	89.931 (2)
<i>V</i> , Å ³	404.792661 (3)	4852.2 (3)
2θ range, °		5–90
Rwp, %		9.06
Rp, %		7.01
RB, %		3.01
χ^2		1.61

uneven edges. A similar plate shape was observed in the synthesis of $\text{Bi}_2\text{Fe}_4\text{O}_9$ by the hydrothermal method with an average grain size of $450\ \mu\text{m}$ [36].

Observed elemental composition of phases: Bi, Sn, Fe, O for $\text{Bi}_2(\text{Sn}_{0.7}\text{Fe}_{0.3})_2\text{O}_7$ (Fig. 3, *a*) and Bi, Fe, O for $\text{Bi}_2\text{Fe}_4\text{O}_9$ (Fig. 3, *b*) indicate good quality of the composite sample. The average grain size is $1\ \mu$ [37].

The magnetoelectric interaction is established from measurements of induced electric polarization in magnetic fields up to 13 kOe. The thermoelectric voltage on the opposite sides of the sample was recorded by Agilent Technologies multimeter 34410A in the temperature range 80–500 K. Studies of electrical properties at direct current were performed by a two-probe method at the Agilent Technologies 34410A installation in the temperature range of 80–400 K.

3. Results and discussion

3.1. Volt-ampere characteristic (VAC)

The voltage-ampere characteristics of BSFO/BFO detect hysteresis (Fig. 4), which is shifted along the current axis as a result of the presence of an uncompensated charge created by defects in the cationic and anionic subsystems. The width of the hysteresis loop of the VAC composite compound practically does not change to 160 K (insert Fig. 4, *a*), from 200 K there is an increase, at $T = 360\ \text{K}$ has the maximum value. The hysteresis acquires a non-symmetrical shape with an increase in temperature, after 360 K. A hysteresis constriction occurs at 390 K, the maximum width of the hysteresis shifts to 100 V and practically disappears with further heating.

The hysteresis of the VAC is due to the ferroelectric polarization of Fig. 4, *b*, created by the Bi-O polar bond with an unshared electron pair on the bismuth ion. The polarization in the mullite is below the Neel temperature, due to the formation of an inhomogeneous magnetic state and an unshielded electron pair on the bismuth ion. Hysteresis in the temperature range 80–160 K is practically absent, at 240–450 K the residual polarization increases exponentially (insert Fig. 4, *b*). The residual polarization in the zero field is due to both stannate and mullite.

According to the literature data [26], ceramic $\text{Bi}_2\text{Fe}_4\text{O}_9$ exhibits ferroelectric properties, at room temperature at a frequency of 10 Hz, a hysteresis loop of electrical polarization is observed. The shape of the loop depends on the grain size. Samples with a grain size of 60 nm have rounded loop ends, which is explained by large leakage currents. When the grain size is more than 200 nm, the P-E loop is not saturated at room temperature. Mullite with a grain size of 900 nm is characterized by residual polarization $P_r = \mu\text{C}/\text{cm}^2$ and coercive field $E_c = 19.5\ \text{kV}/\text{cm}$ in electric field 60 kV/cm [26]. In other sources [27] it is reported that at room temperature, due to leakage currents, ferroelectric hysteresis is not detected. The P-E loop is

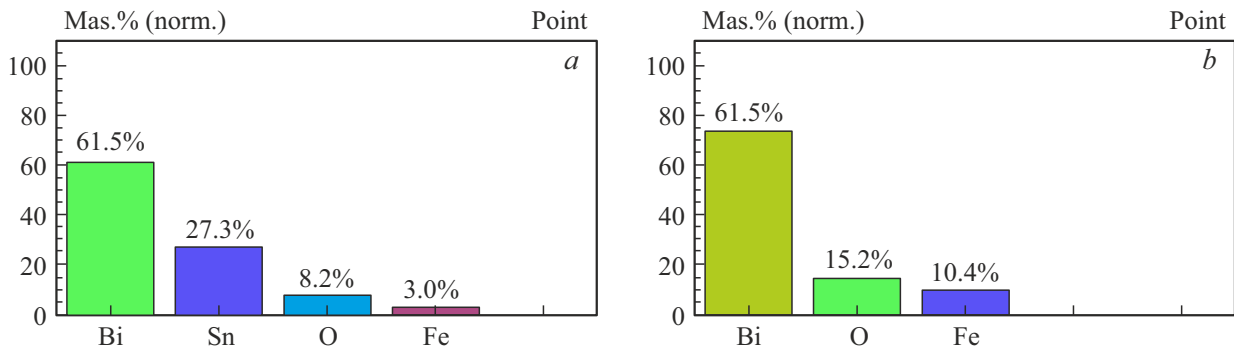


Figure 3. The elemental composition of the phases of the composite $\text{Bi}_2(\text{Sn}_{0.7}\text{Fe}_{0.3})_2\text{O}_7/\text{Bi}_2\text{Fe}_4\text{O}_9$: *a* — $\text{Bi}_2(\text{Sn}_{0.7}\text{Fe}_{0.3})_2\text{O}_7$, *b* — $\text{Bi}_2\text{Fe}_4\text{O}_9$.

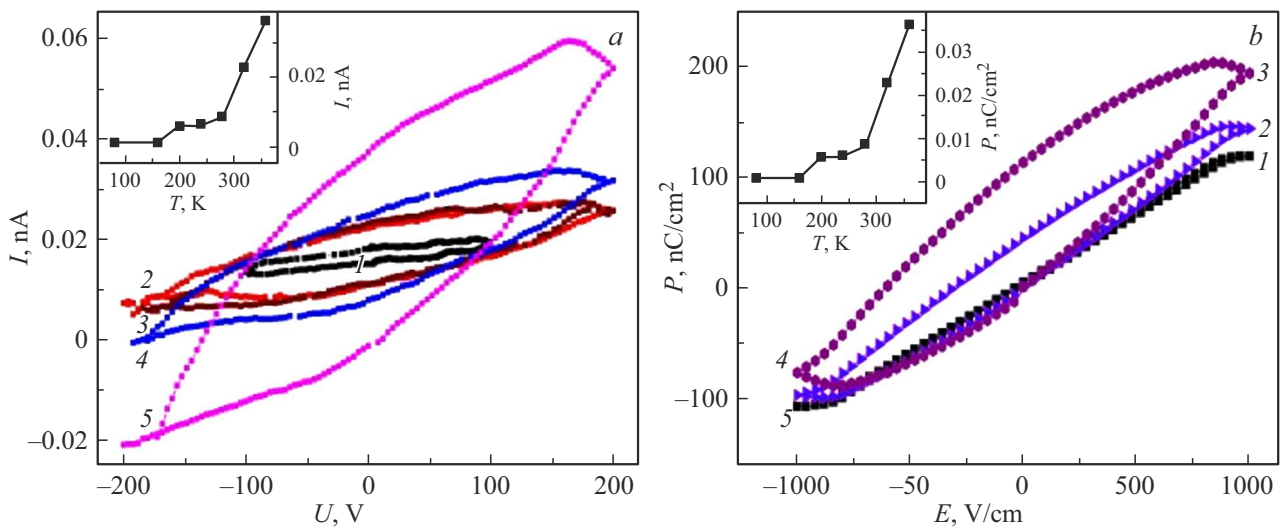


Figure 4. *a* — volt-ampere characteristic $\text{Bi}_2(\text{Sn}_{0.7}\text{Fe}_{0.3})_2\text{O}_7/\text{Bi}_2\text{Fe}_4\text{O}_9$ at different temperatures. The curve 1 corresponds to $T = 80$, 2 — 200, 3 — 240, 4 — 280, 5 — 320 K. The insert shows the temperature dependence of the hysteresis width of the VAC $\text{Bi}_2(\text{Sn}_{0.7}\text{Fe}_{0.3})_2\text{O}_7/\text{Bi}_2\text{Fe}_4\text{O}_9$. *b* — field dependence of polarization $\text{Bi}_2(\text{Sn}_{0.7}\text{Fe}_{0.3})_2\text{O}_7/\text{Bi}_2\text{Fe}_4\text{O}_9$ at different temperatures. The curve 1 corresponds to $T = 80$, 2 — 300, 3 — 360 K. The insert shows the temperature dependence of the residual polarization $\text{Bi}_2(\text{Sn}_{0.7}\text{Fe}_{0.3})_2\text{O}_7/\text{Bi}_2\text{Fe}_4\text{O}_9$.

observed at low temperatures $T = 250$ K, at a frequency of 1 Hz, in the region of the magnetic ordering of the mullite.

3.2. Magnetoelectric effect

The magnetoelectric interaction BSFO/BFO is established from the induced electric polarization in the magnetic field. Figure 5 shows the field dependence of polarization at temperatures 100, 240, 280 and 380 K. The parameter of the magnetoelectric interaction changes sign in the region of the temperature of the magnetic transition in the mullite.

The polarization induced by the magnetic field is described as

$$P = aH + b \frac{H^2}{1 + dH^2}, \quad (1)$$

where a , b , d — matching parameters. The magnetoelectric interaction is due to the spin-orbit interaction with a linear dependence on the field and with a quadratic dependence on the field.

In the temperature range of 100–240 K, the polarization is an odd function of the magnetic field associated with the inhomogeneous magnetic state of the mullite. In work [38] it was found that $\text{Bi}_2\text{Fe}_4\text{O}_9$ is characterized by a non-collinear antiferromagnetic ordering of spins with a ferromagnetic order by one of the spin components.

In the temperature range 225–235 K there is an anomaly $\chi(T)$ in the composite compound BSFO/BFO, which is caused by a magnetic phase transition in $\text{Bi}_2\text{Fe}_4\text{O}_9$ from antiferromagnetic to paramagnetic state. The value of the residual magnetization during heating decreases fourfold to $T = 100$ K with a further increase of 6 times [37]. The field dependence of the BSFO/BFO magnetization in the temperature range 4–300 K detects hysteresis. This magnetic behavior of the composite is explained in the model of magnetic polarons in an antiferromagnetic matrix, taking into account the orbital angular magnetic moments. A single electron can create a ferromagnetic micro-region

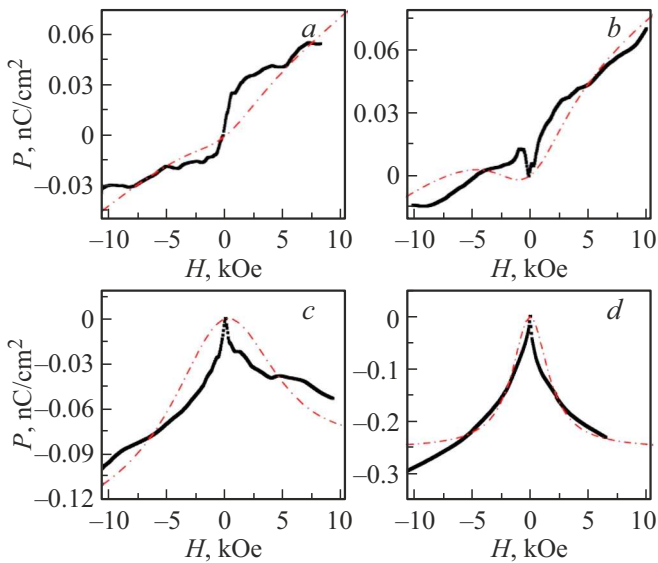


Figure 5. Field dependence of polarization $\text{Bi}_2(\text{Sn}_{0.7}\text{Fe}_{0.3})_2\text{O}_7/\text{Bi}_2\text{Fe}_4\text{O}_9$ at different temperatures. The dashed lines correspond to the theoretical calculations according to the formula (1). *a* — $T = 100$, *b* — 240 , *c* — 280 , *d* — 380 K.

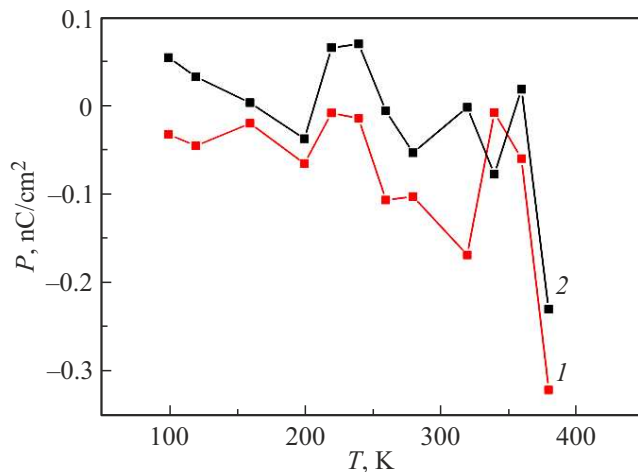


Figure 6. Temperature dependence of polarization $\text{Bi}_2(\text{Sn}_{0.7}\text{Fe}_{0.3})_2\text{O}_7/\text{Bi}_2\text{Fe}_4\text{O}_9$. The curve 1 corresponds to polarization measured in a positive magnetic field, 2 — negative magnetic field.

and localize in it, forming a ferron. The ferromagnetic micro-region (ferron radius) is determined by the competition between the kinetic energy of charge carriers and the exchange energy of localized spins. Impurity electrons as a result of the $s-d$ interaction induce a non-collinear configuration of spins in the micro-region. The exchange energy decreases with heating as a result of a decrease in the correlation between the directions of neighboring spins. When heated, the radius of the ferrons increases and as a result of the interaction between electrons trapped by oxygen vacancies, the formation of weak magnetization [39] is possible.

Polarization in the BSFO/BFO composite is an odd function of the magnetic field in the vicinity of the $\alpha \rightarrow \beta$ structural transition at 360 K and is caused by the accumulation of charged defects at the crystallographic boundaries. In bismuth pyrostannate $\text{Bi}_2\text{Sn}_2\text{O}_7$ $\alpha \rightarrow \beta$ the transition is realized at $T = 400$ K [30]. The transition temperature shifts towards low temperatures with an increase in the concentration of iron ions. The transition is observed in $\text{Bi}_2(\text{Sn}_{0.8}\text{Fe}_{0.2})_2\text{O}_7$ $\alpha \rightarrow \beta''$ at 350 K [40]. Bismuth pyrostannate $\text{Bi}_2(\text{Sn}_{0.8}\text{Fe}_{0.2})_2\text{O}_7$ has a non-centrosymmetric distorted structure [40], which creates prerequisites for the occurrence of electric polarization and, as a consequence, magnetoelectric the [41] effect.

The linear magnetoelectric effect decreases with increasing temperature, so at a temperature of 100 K the magnitude of the linear component is $5.6 \cdot 10^{-12}$, $4 \cdot 10^{-12}$ at $T = 240$ K, $1.8 \cdot 10^{-12}$ at $T = 280$ K and disappears at $T = 380$ K. A linear magnetoelectric effect is possible in crystals without a center of symmetry in the paramagnetic phase. For example, in ytterbium molecular complexes, ytterbium ions in an external magnetic field induce electric polarization [42]. The linear longitudinal magnetoelectric effect detected in a single crystal $\alpha - \text{Bi}_2\text{O}_3$ was attributed to paramagnetic centers [43]. This effect is caused by the formation of a quasi-gap in the electronic excitation spectrum of bismuth oxides. In two-dimensional materials (2D Dirac), for example MoS_2 , the linear magnetoelectric effect is associated with the presence of „valleys“ in the spectrum of electronic excitations [44]. These results agree well with the theoretical model of „valleys“ described by the topological invariant of the Berry curvature [44].

Figure 6 shows the temperature dependence of the magnetoelectric effect in the magnetic field +10 kOe (curve 1) and -10 kOe. The curves have a non-linear appearance, in the region of the magnetic transition in the mullite $\text{Bi}_2\text{Fe}_4\text{O}_9$ a wide maximum is manifested.

3.3. Thermopower

Figure 7 shows the temperature dependence of the BSFO/BFO thermal EMF coefficient in the temperature range 80–520 K when heated. The value $\alpha(T)$ at temperatures 253 and 310 K changes sign, which indicates a change in the type of current carriers.

The maximum in absolute value on the temperature dependence of the thermal emf coefficient in the region of 115 K is explained by the structural phase transition in bismuth pyrostannate $\text{Bi}_2(\text{Sn}_{0.7}\text{Fe}_{0.3})_2\text{O}_7$. Substitution of ions Sn^{4+} with ions Fe^{3+} induces distortions of the crystal structure, and an increase in the concentration of ions Fe^{3+} leads to phase transitions of the displacement type. Thus, in $\text{Bi}_2(\text{Sn}_{1-x}\text{Fe}_x)_2\text{O}_7$ with concentrations $x = 0.2$ at $T = 140$ K a transition from monoclinic to triclinic symmetry [40]. The shift of the phase transition temperature in the BSFO/BFO composite towards lower temperatures depends on two factors. This is an increase

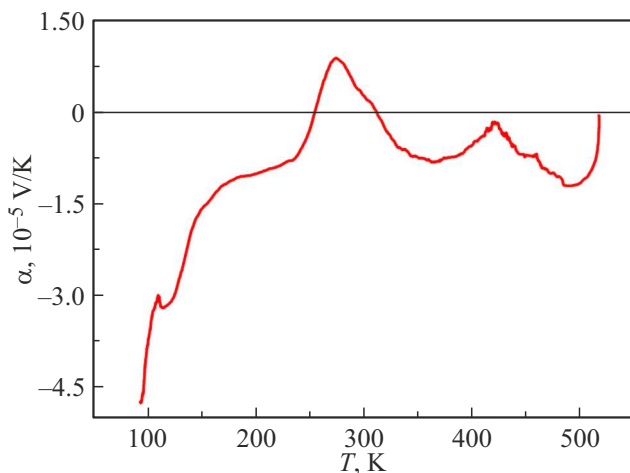


Figure 7. Temperature dependence of thermopower of $\text{Bi}_2(\text{Sn}_{0.7}\text{Fe}_{0.3})_2\text{O}_7/\text{Bi}_2\text{Fe}_4\text{O}_9$.

in the concentration of Fe^{3+} and the coexistence of two crystal structures with different spatial groups.

A wide anomaly is observed on the curve $\alpha(T)$ at the temperature $T = 366$ K. This temperature correlates with the data of the ME effect and is consistent with the beginning of the $\alpha \rightarrow \beta$ transition in bismuth pyro-stannate. The maximum in absolute value on the curve $\alpha(T)$ in the range 480–515 K is caused by a structural transition associated with the disappearance of the inversion center in bismuth pyrostannate.

The value of the thermo-emf is predominantly negative. Iron-substituted bismuth pyrostannate $\text{Bi}_2(\text{Sn}_{0.8}\text{Fe}_{0.2})_2\text{O}_7$ does not change the type of conductivity over the entire temperature range and has a positive thermal EMF value [45]. The change in the sign of the thermal EMF coefficient for iron concentration is probably due to the growth of oxygen vacancies in the composite, which is confirmed by an increase in the residual magnetization of mullite in the bismuth pyro-stannate matrix compared with polycrystalline mullite [37].

4. Conclusion

The hysteresis of the VAC and the maximum value of the hysteresis width in the region α – β of the transition in bismuth pyro-stannate and its further disappearance were found. The relationship of the hysteresis of the BSFO/BFO composite with the ferroelectric polarization of the mullite is determined.

The magnetoelectric effect is detected and the temperature regions of the predominance of the odd function of the magnetic field are found. The temperature of disappearance of the linear magnetoelectric effect in the β -phase $\text{Bi}_2(\text{Sn}_{0.7}\text{Fe}_{0.3})_2\text{O}_7$ was determined.

A change in the sign of the thermopower associated with structural transitions has been established.

Funding

The work was carried out within the framework of the scientific topic of the State Assignment of the Institute of Physics of the Siberian Branch Russian Academy of Sciences.

Conflict of interest

The authors declare that they have no conflict of interest.

References

- [1] E. Jartych, T. Pikula, K. Kowal, J. Dzik, P. Guzdek, D. Czekaj. *Nanoscale Res. Lett.* **11**, 234 (2016).
- [2] M.I. Bichurin, V.M. Petrov, R.V. Petrov, Y.V. Kiliba, F.I. Bukashev, A.Y. Smirnov, D.N. Eliseev. *Ferroelectr.* **280**, 199 (2002).
- [3] N.H. Duc, D.T. Huong Giang. *J. Alloy Compd.* **449**, 214 (2008).
- [4] D.T. Huong Giang, N.H. Duc. *Sensor Actuat. A-Phys.* **149**, 229 (2009).
- [5] S. Dong, J. Zhai, J.F. Li, D. Viehland, S. Priya. *Appl. Phys. Lett.* **93**, 103511 (2008).
- [6] X. Bai, Y. Wen, J. Yang, P. Li, J. Qiu, Y. Zhu. *J. Appl. Phys.* **111**, 07A938 (2012).
- [7] G. Srinivasan, S. Priya, N. Sun. *Composite magnetoelectrics: materials, structures, and applications*. Woodhead Publishing, Cambridge. (2015). 380 p.
- [8] M. Bibes, A. Barthelemy. *Nature Mater* **7**, 425 (2008).
- [9] J. Hu, Z. Li, J. Wang, C.W. Nan. *J. Appl. Phys.* **107**, 093912 (2010).
- [10] Z. Shi, C. Wang, X. Liu, C. Nan. *Chinese Sci. Bull.* **53**, 2135 (2008).
- [11] S. Fusil, V. Garcia, A. Barthelemy, M. Bibes. *Annu Rev. Mater. Res.* **44**, 91 (2014).
- [12] M. Gajek, M. Bibes, S. Fusil, K. Bouzehouane, J. Fontcuberta, A. Barthélémy, A. Fert. *Nature Mater.* **6**, 296 (2007).
- [13] L.W. Martin, Y.H. Chu, Q. Zhan, R. Ramesh, S.J. Han, S.X. Wang, M. Warusawithana, D.G. Schlom. *Appl. Phys. Lett.* **91**, 172513 (2007).
- [14] G. Catalan, J.F. Scott. *Adv Mater.* **21**, 2463 (2009).
- [15] J. Wang, J.B. Neaton, H. Zheng, V. Nagarajan, S.B. Ogale, B. Liu, D. Viehland, V. Vaithyanathan, D.G. Schlom, U.V. Waghmare, N.A. Spaldin, K.M. Rabe, M. Wuttig, R. Ramesh. *Science* **299**, 1719 (2003).
- [16] J.P. Rivera. *J. Eur. Phys. B* **71**, 299 (2009).
- [17] J. Ryu, A.V. Carazo, K. Uchino, H.E. Kim. *Jpn J. Appl. Phys.* **40**, 4948 (2001).
- [18] U. Laletsin, N. Padubnaya, G. Srinivasan, C.P. DeVreugd. *Appl. Phys. A* **78**, 33 (2004).
- [19] T.C. Han, W.L. Hsu, W.D. Lee. *Nanoscale Res. Lett.* **6**, 201 (2011).
- [20] M.D. Gerngross, J. Carstensen, H. Föll. *Nanoscale Res. Lett.* **7**, 379 (2012).
- [21] X. Liu, S. Liu, M.G. Han, L. Zhao, H. Deng, J. Li, Y. Zhu, L. Krusin-Elbaum, S. O'Brien. *Res. Lett.* **8**, 374 (2013).
- [22] A.A. Bukharaev, A.K. Zvezdin, A.P. Pyatakov, Yu.K. Fetisov. *UFN* **188**, 12, 1288 (2018). (in Russian).
- [23] A. Kirsch, M.M. Murshed, F.J. Litterst, T.M. Gesing. *J. Phys. Chem. C* **123**, 5, 3161 (2019).

- [24] H. Koizumi, N. Niizeki, T. Ikeda. *Jpn. J. Appl. Phys.* **3**, 495 (1964).
- [25] N.I. Zakharchenko. *Russ. J. Appl. Chem.* **73**, 2047 (2000).
- [26] Z.M. Tian, S.L. Yuan, X.L. Wang, X.F. Zheng, S.Y. Yin, C.H. Wang, L. Liu. *J. Appl. Phys.* **106**, 103912 (2009).
- [27] A.K. Singh, S.D. Kaushik, B. Kumar, P.K. Mishra, A. Venimadhav, V. Siruguri, S. Patnaik. *Appl. Phys. Lett.* **92**, 132910 (2008).
- [28] M. Kumar, K.L. Yadav. *J. Appl. Phys.* **100**, 074111 (2006).
- [29] Hui Shen, Li Shen, Zhonghai Lin, Meihua Li, Yanli Liu. *J. Alloys Compd.* **924**, 166535 (2022).
- [30] L.V. Udod, S.S. Aplesnin, M.N. Sitnikov, M.S. Molokeev. *FTT* **56**, 7, 1315 (2014).
- [31] L. Udod, S. Aplesnin, M. Sitnikov, O. Romanova, O. Bayukov, A. Vorotinov, D. Velikanov, G. Patrin. *Eur. Phys. J. Plus.* **135**, 776 (2020).
- [32] I.A. Verbenko, L.A. Reznichenko. *Innovation and expertise* **1**, 12, 40 (2014). (in Russian).
- [33] A.P. Pyatakov, A.K. Zvezdin. *UFN* **182**, 6, 593 (2012). (in Russian).
- [34] M.K. Verma, V. Kumar, T. Das, R.K. Sonwani, V.S. Rai, D. Prajapati, K. Sahoo, V.K. Kushwaha, A. Gupta, K. Mandal. *J. Miner. Mater. Char. Eng.* **9**, 444 (2021).
- [35] Bruker AXS TOPAS V4: General profile and structure analysis software for powder diffraction data. — User's Manual. Bruker AXS, Karlsruhe, Germany, 2008.
- [36] Jian-Tao Han, Yun-Hui Huang, Rui-Jie Jia, Guang-Cun Shan, Rui-Qian Guo, Wei Huang. *J. Cryst. Growth* **294**, 469 (2006).
- [37] S.S. Aplesnin, L.V. Udod, M.N. Sitnikov, D.A. Velikanov, M.N. Molokeev, O.B. Romanova, A.V. Shabanov. *JMMM* **559**, 169530 (2022).
- [38] K. Jindal, Sh. Ameer, M. Tomar, P.K. Jha, V. Gupta. *Mater. Today: Proc.* **47**, 8, 1637 (2021).
- [39] M.Yu. Kagan, K.L. Kugel. *UFN* **171**, 577 (2001). (in Russian).
- [40] L.V. Udod, S.S. Aplesnin, M.N. Sitnikov, O.B. Romanova, M.N. Molokeev. *J. Alloys Compd.* **804**, 281 (2019).
- [41] A.K. Zvezdin, A.P. Pyatakov. *UFN* **179**, 887 (2009). (in Russian).
- [42] Jérôme Long, M.S. Ivanov, V.A. Khomchenko, E. Mamonova, Jean-Marc Thibaud, Jérôme Rouquette, Mickaël Beaudhuin, Dominique Granier, Rute A.S. Ferreira, Luis D. Carlos, Bruno Donnadieu, Marta S.C. Henriques, José António Paixão, Yannick Guari, J. Larionova. *Science* **367**, 671 (2020).
- [43] V.I. Nizhankovskii, A.I. Kharkovskii, V.G. Orlov. *Ferroelectrics* **279**, 157 (2002).
- [44] Jieun Lee, Zefang Wang, Hongchao Xie, Kin Fai Mak, Jie Shan. *Nature Mater.* **16**, 887 (2017).
- [45] S.S. Aplesnin, L.V. Udod, M.N. Sitnikov, O.B. Romanova. *Ceram. Int.* **47**, 1704 (2021).

Translated by A.Akhtyamov